Progress In Electromagnetics Research, Vol. 111, 467–481, 2011

DESIGN OF SUBWAVELENGTH TUNABLE AND STEERABLE FABRY-PEROT/LEAKY WAVE ANTENNAS

F. Costa and A. Monorchio

Department of Information Engineering
University of Pisa, Via Caruso 16, Pisa 56122, Italy

Abstract—The design of a thin tunable and steerable Fabry-Perot antenna is presented. The subwavelength structure is analyzed both by an efficient transmission line model and by full-wave simulations. The tunable antenna consists of a low profile resonant cavity made up of a Partially Reflecting Surface (PRS) placed in close proximity of a tunable high-impedance surface. The active ground plane is synthesized by loading the high-impedance surface with varactor diodes. Such design allows both tuning the high-gain operational frequency and obtaining a beam steering/shaping for each resonant frequency. The transmission line model here presented includes averaged analytical expressions for modelling the tunable high-impedance surface and the partially reflecting surface. All the theoretical speculations are verified by full-wave simulations on a finite size structure.

1. INTRODUCTION

A Fabry-Perot antenna can be realized by placing a highly reflective frequency selective surface at a proper distance from a ground plane. The cavity, excited by a low gain antenna, converts an omnidirectional field distribution into a highly directive one [1]. Such structure is often addressed also as leaky wave antenna since its radiation mechanism can be also interpreted in terms of leaky waves [2–4]. When the topic of metamaterial started to attract more attention, this kind of antenna has been also interpreted as a lens based on a zero permittivity superstrate [5, 6]. In the last ten years, many authors analyzed the interesting properties of this antenna trying to improve its efficiency, bandwidth and thickness. Regarding the

Received 17 November 2010, Accepted 23 December 2010, Scheduled 24 December 2010
Corresponding author: Filippo Costa (filippo.costa@iet.unipi.it).

thickness reduction, important improvements have been obtained. In the case of a metallic ground plane, the cavity height equals $\lambda/2$ [7]. In 2005 Feresidis et al. presented a novel configuration where the electric ground plane was replaced by an artificial magnetic conductor [8, 9]. This design calls for a cavity with a halved thickness with respect to the original configuration. Such configuration was further improved by exploiting a High-Impedance Surface (HIS) with a generic negative phase response [10–12].

An interesting evolution of this structure is the transformation of the antenna in a reconfigurable radiator. Indeed, the employment of a tunable HIS [13, 14] in place of a static one allows the structure operating for different frequencies [15]. In this configuration, the employment of a tunable primary radiator could be necessary for maintaining the impedance matching [16, 17]. According to the leaky wave principles, a beam steering can also be obtained for every working frequency by dynamically varying the phase response of the ground plane (it determines a fictitious variation of the cavity height).

In this paper, a transmission line model (TL) [18] for analyzing the radiation patterns is combined with an exhaustive analytical model for high-impedance surfaces [19]. This analytical approach allows also to consider the angular dependence of the HIS response in computing the radiation pattern of the structure and the presence of active elements.

2. FORMULATION

The layout of the analyzed structure and its equivalent transmission line circuit are shown in Fig. 1.

The antenna is analyzed by a transmission line approach in which the source is assumed to be a horizontal infinitesimal electric dipole inside the resonant Fabry-Perot cavity [20]. The original problem of analyzing the far field radiation of the Hertzian dipole inside the cavity is transformed into a scattering problem. Thus, the calculation reduces to a calculation of the field in the position of the source dipole due to an incident plane-wave. In the equivalent TL approach, this corresponds to determining the voltage V_x in correspondence of the dipole position. The voltage V_x is computed by solving the following system of equations [18]:

$$\begin{aligned} \begin{bmatrix} V_s - I_N R_s \\ I_N \end{bmatrix} &= \begin{bmatrix} A & B \\ C & D \end{bmatrix} \begin{bmatrix} I_0 Z_{HIS} \\ I_0 \end{bmatrix} \\ \begin{bmatrix} V_x \\ I_x \end{bmatrix} &= \begin{bmatrix} A' & B' \\ C' & D' \end{bmatrix} \begin{bmatrix} I_0 Z_{HIS} \\ I_0 \end{bmatrix} \end{aligned} \tag{1}$$

where I_N is the current in the N-th transmission line, V_s is the source

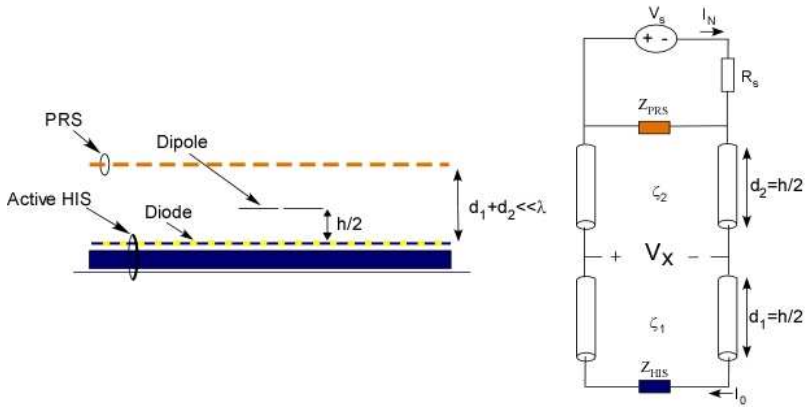

Figure 1. (a) Layout of the analyzed structure and (b) equivalent circuit.

voltage, R_s represents the free space impedance and A, B, C, D constitute the chain matrix of the whole system. Such matrix can be computed as product of the three matrices composing the system:

$$\begin{bmatrix} A & B \\ C & D \end{bmatrix} = [M_{PRS}]\,[M_2]\,[M_1] \tag{2}$$

with

$$[M_n] = \begin{bmatrix} \cos(k_{zn}d_n) & jZ_{cn}\sin(k_{zn}d_n) \\ j\frac{\sin(k_{zn}d_n)}{Z_{cn}} & \cos(k_{zn}d_n) \end{bmatrix} \quad [M_{PRS}] = \begin{bmatrix} 1 & 0 \\ 1/Z_{PRS} & 1 \end{bmatrix} \tag{3}$$

where Z_{PRS} represents the lumped impedance of the partially reflecting surface (its expression is given below). The matrix A', B', C', D', representing the chain matrix of the transmission line between the source and the load impedance Z_{HIS}, is equal to M_1. The voltage can be computed both for TE and TM polarization by employing the following relations:

$$\begin{aligned} k_{zn} &= k_0\sqrt{\varepsilon_{rn} - \sin^2(\vartheta_i)} \\ Z_{cn}^{TE} &= \frac{\eta_0}{\sqrt{\varepsilon_{rn} - \sin^2(\vartheta_i)}}, \quad Z_{cn}^{TM} = \frac{\eta_0\sqrt{\varepsilon_{rn} - \sin^2(\vartheta_i)}}{\varepsilon_{rn}} \\ R_s^{TE} &= Z_0^{TE} = \eta_0/\cos(\vartheta_i), \quad R_s^{TM} = Z_0^{TM} = \eta_0\cos(\vartheta_i) \\ V_S^{TE} &= 1, \quad V_S^{TM} = V_S^{TE}\cos(\vartheta_i) \end{aligned} \tag{4}$$

By solving the system in (1), the following equation for the voltage is provided [18]:

$$V_x = V_s \frac{A' Z_{HIS} + B'}{C Z_{HIS} R_S + D R_S + A Z_{HIS} + B} \tag{5}$$

Once computed the voltage for TE and TM polarization, the radiation patterns can be obtained on both E plane and H plane by normalizing the absolute value of the field magnitude to its maximum. The expression of the field components in the two main planes are:

$$H\text{-plane } (\phi = 90^\circ) : |E_\phi| = \left|V_x^{TE}\right|; \quad E\text{-plane } (\phi = 0^\circ) : |E_\vartheta| = \left|V_x^{TM}\right| \tag{6}$$

The impedance of the partially reflecting surface, Z_{PRS}, is not assumed constant with the incident angle as in [20] but it is defined according to the averaged boundary condition theory [21]. In this approach, the impedance is derived assuming an average current on the plane of the wires including the frequency selective surface. By applying the Babinet theorem, the surface impedance of an array of patches is obtained as well. These expressions are valid both for normal and oblique incidence under the hypothesis of homogeneous array ($D < \lambda/3$). In the present work, the PRS on the top of the cavity consists of an inductive grid and its impedance reads [21]:

$$\begin{aligned} Z_{PRS,grid}^{TE} &= j \tfrac{\omega \mu_0 D}{2\pi} \ln\left(\tfrac{1}{\sin\left(\frac{\pi w}{2D}\right)}\right) \\ Z_{PRS,grid}^{TM} &= j \tfrac{\omega \mu_0 D}{2\pi} \left(1 - \tfrac{k_0}{k_{eff}} \tfrac{\sin^2(\vartheta_i)}{2}\right) \ln\left(\tfrac{1}{\sin\left(\frac{\pi w}{2D}\right)}\right) \end{aligned} \tag{7}$$

where $k_{eff} = k_0 \sqrt{\varepsilon_{eff}}$ is the wave number of the incident wave vector in the effective host medium, $\varepsilon_{eff} = (\varepsilon_{up} + \varepsilon_{down})/2$ represents the effective permittivity of an equivalent uniform medium composed by the two dielectrics surrounding the grid, D is the grid period, w is the strip width and μ_0, k_0 are, respectively, the permeability and the wave number in free space.

The load impedance in the equivalent circuit represents the surface impedance of the high-impedance surface. Such impedance, computed by the parallel connection between the impedance of the grounded dielectric slab and the grid impedance of a patch array, reads [19]:

$$Z_{HIS}^{TE} = \frac{j\omega\mu_0 \frac{\tan(k_z d_{HIS})}{k_z}}{1 - k_0^2 (1+\varepsilon_{rHIS}) \frac{P}{\pi} \ln\left(\frac{1}{\sin\left(\frac{\pi g}{2P}\right)}\right) \frac{\tan(k_z d_{HIS})}{k_z} \left(1 - \frac{\sin^2(\vartheta_i)}{1+\varepsilon_{rHIS}}\right)} \tag{8}$$

$$Z_{HIS}^{TM} = \frac{j\omega\mu_0 \frac{\tan(k_z d_{HIS})}{k_z}\left(1-\frac{\sin^2(\vartheta_i)}{\varepsilon_{rHIS}}\right)}{1-k_0^2\left(1+\varepsilon_{rHIS}\right)\frac{P}{\pi}\ln\left(\frac{1}{\sin\left(\frac{\pi g}{2P}\right)}\right)\frac{\tan(k_z d_{HIS})}{k_z}\left(1-\frac{\sin^2(\vartheta_i)}{\varepsilon_{rHIS}}\right)} \quad (9)$$

where P is the periodicity of the patch array, g is the gap width between patches, ε_{rHIS} and d_{HIS} are the permittivity and the thickness of the dielectric slab composing the HIS, $k_z = \sqrt{k^2 - k_t^2}$ is the propagation constant along the normal of the slab and $k_t = k_0 \sin(\vartheta)$ is the transverse wavenumber.

The analysis of the tunable high-impedance surface is performed by adding an additional lumped capacitor, in parallel with the capacitance created by the patch array [14]. If we represent the impedance of the capacitive patch array comprising the high-impedance surface as a lumped capacitor ($Z_{patch}^{TE/TM} = 1/j\omega C_{patch}$), the introduction of the diode is done by placing the lumped element impedance in parallel to the FSS impedance. As is well known, a varactor diode can be represented as a series of a resistor and a capacitor. The new capacitance of the patch array is well approximated also by neglecting the presence of the series resistance (considering realistic values below $10\,\Omega$) of the diode:

$$C_{patch\_active}^{TE} \simeq C_{var} + \frac{P\varepsilon_0\left(1+\varepsilon_{rHIS}\right)}{\pi}\ln\left(\frac{1}{\sin\left(\frac{\pi g}{2P}\right)}\right)\left(1-\frac{k_0}{k_{eff}}\frac{\sin^2(\vartheta_i)}{2}\right) \quad (10)$$

$$C_{patch\_active}^{TM} \simeq C_{var} + \frac{P\varepsilon_0\left(1+\varepsilon_{rHIS}\right)}{\pi}\ln\left(\frac{1}{\sin\left(\frac{\pi g}{2P}\right)}\right) \quad (11)$$

where C_{var} represents the variable capacitance of the diode. The losses of the varactor, taken into account by the series resistor R_{var}, can be included within the real part of the new patch array impedance as follows:

$$R_{patch\_active}^{TE,TM} = \frac{R_{var}C_{var}^2}{R_{var}^2 C_{var}^2 C_{patch}^2 + \left(C_{var}+C_{patch}\right)^2} \simeq \frac{R_{var}C_{var}^2}{\left(C_{var}+C_{patch}\right)^2} \quad (12)$$

The simplified equivalent circuit of the active capacitive FSS is reported in Fig. 2. If the capacitance of the varactor is of the same order of magnitude of the patch array capacitance, the effect of the diode resistor as a series FSS resistance is equivalent to a resistor of $1/4 \cdot R_{var}$. At this stage, the losses of the high-impedance ground plane can be studied as ones of a HIS composed by a resistive FSS [22].

In the full-wave simulations, these lumped varactors are connected between all the neighbouring patches.

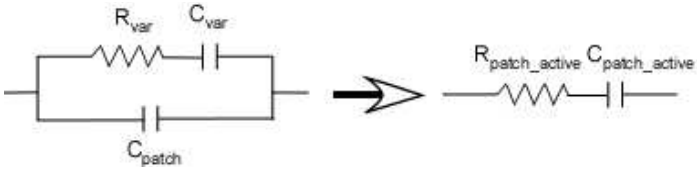

Figure 2. Modelization of the patch array FSS loaded with varactors which comprises the high-impedance ground plane.

3. TUNABLE AND STEERABLE ANTENNA DESIGN

By employing the active high-impedance surface it is possible to obtain a tunable and steerable subwavelength cavity antenna. Indeed, the operative frequency of the cavity can be approximately determined through the ray optic analysis as:

$$f = \frac{c}{4h\pi}\left[\phi_R + \psi_R + 2n\pi\right], \; n = 0, 1, 2 \ldots \tag{13}$$

where h is the height of the cavity, Φ_R is the phase reflection coefficient of the PRS and ψ_R represents the phase reflection coefficient of the artificial ground plane. By varying the reflection phase of the HIS, the operating frequency of the cavity can be varied. Moreover, the cavity height h results to be much smaller than a half wavelength since the phase of the high-impedance surface assumes a generic negative value.

A change of the cavity height, by keeping constant the working frequency, leads to a beam steering. This antenna, under the assumption that the ground plane and the PRS behaves as a PEC interface, can be seen as a leaky parallel-plate waveguide operating in the $n = 1$ mode [20]. Considering that the phase of the ground plane reflection can be changed by employing a HIS ground plane and the phase of the PRS is not exactly equal to π, the radiation angle θ of the antenna can be obtained as follows:

$$\vartheta = \cos^{-1}\left[\frac{\lambda}{4\pi h}\left(\phi_R + \psi_R + 2n\pi\right)\right], \; n = 0, 1, 2 \ldots \tag{14}$$

In order to show the validity of these arguments, the formulas previously presented are used for analyzing an example of a tunable and steerable antenna.

A PRS has been designed as a planar inductive grid with a periodicity of 22 mm and a strip width of 8 mm. In order to get a more reliable practical design, a supporting dielectric for the PRS has been considered. The dielectric has a thickness of 3.2 mm with a relative permittivity equal to 2.55-j0.0048. The height of the cavity

is equal to 13 mm, which roughly corresponds to $\lambda_0/7$ at the chosen operating frequency of 3.4 GHz. The high-impedance surface consists of a patch array printed on a grounded dielectric slab with the same characteristics of the one supporting the PRS. The patch array is characterized by a periodicity of 15 mm and a gap between the patches of 1 mm. In Fig. 3, the reflection coefficient of the high-impedance ground plane is computed as a function of the varactor capacitance. The diode losses are considered by the series resistance R_{var} with a realistic value of 1 Ω. It has to be pointed out that the cavity does not work in correspondence of the minima of the reflection amplitude observed in Fig. 3(b) but it works for a frequency with a negative phase response, namely after the resonance.

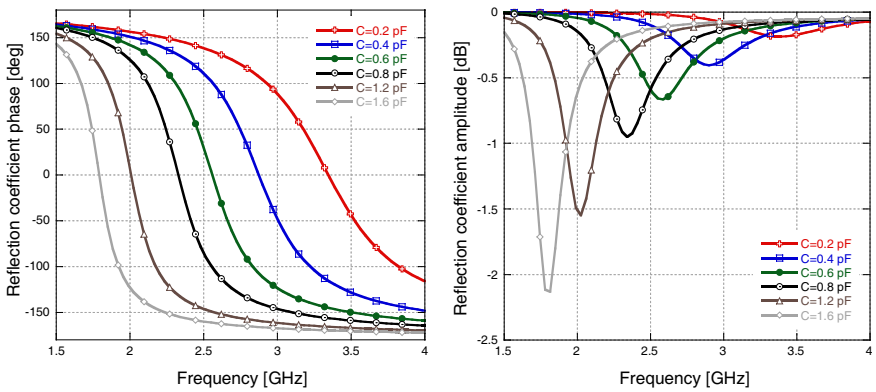

Figure 3. (a) Reflection coefficient phase and (b) reflection coefficient magnitude of the high-impedance ground plane as a function of the varactor capacitance. The losses of the dielectric substrate and a diode resistance of 1 Ω have been considered in the calculation.

In Fig. 4, the radiation patterns of the structure are shown at the operating frequency of 3.42 GHz, varying the diode capacitance. As expected, this electronic variation leads to a fictitious variation of the cavity height and a consequent steering of the beam. Moreover, this active configuration can be used to change the operating frequency of the antenna because, when the diodes polarization is changed, the broadside operating frequency shifts towards lower values.

In Fig. 5, the directivity towards the broadside direction of the antenna is shown for different polarizations of the active elements. This figure shows that the variation of the capacitance value leads to a shift of the maximum broadside directivity. Indeed, when the capacitance value is increased, the reflection phase value of the high-impedance surface at a given frequency decreases, leading to an equivalent higher

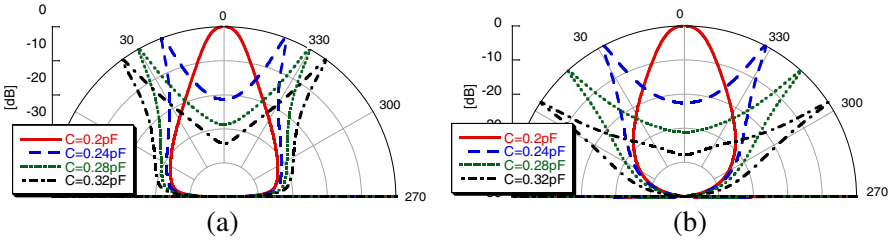

Figure 4. Radiation patterns on the (a) E-pane and (b) H-plane at 3.42 GHz obtained by varying diode capacitances.

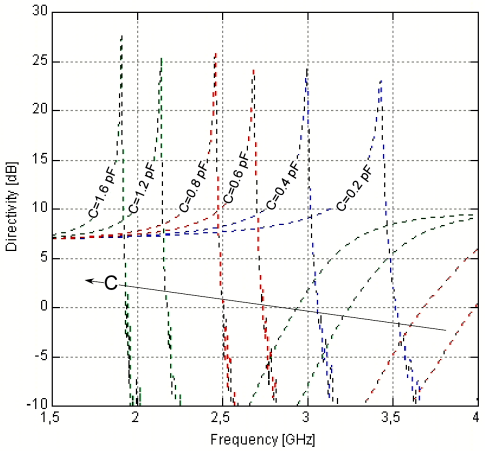

Figure 5. Directivity towards the broadside direction by varying diode capacitances.

cavity height. By employing realistic ranges of capacitance attainable with commercial varicap diodes (i.e., 0.2 pF $\div$ 1.6 pF), a wide range of tunability of the structure is obtained. Indeed, the operation frequency of the antenna spans an octave of bandwidth. The radiation patterns in correspondence of the directivity maxima are pencil beam and the beam steering can be obtained for every frequency by simply varying the diode capacitance around the value that generates the broadside pattern. The matching of the dipole antenna exciting the cavity over all the frequency range can be obtained by exploiting the typical sharp resonance generated by the resonance of the cavity on the input impedance of the dipole [23, 24].

The transmission line model here described allows to analyze the dependence of the radiation patterns on the angular stability of the HIS and of the top PRS layer response. In Fig. 6, the radiation patterns on

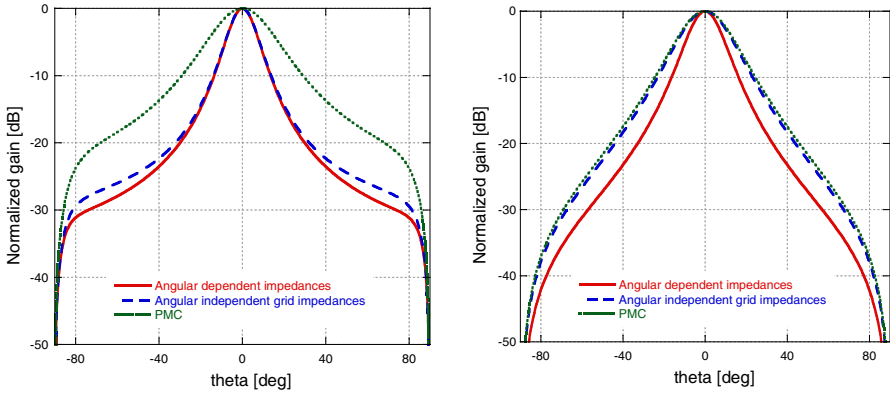

Figure 6. Radiation pattern of the antenna on E and H plane with and without an angular stable impedance. The radiation pattern is computed at 3.4 GHz with a capacitance of the varactor equals to 0.2 pF.

the E and H plane are shown when the angular dependence of the PRS impedances (both the grid impedance of the top layer and the patch array impedance) and of the HIS impedance is considered or not. The latter case is called PMC case since it assumes the HIS impedance angular independent. When the angular dependence of the FSSs is included in the model the radiation pattern of the antennas is more directive than the other two cases. The angular dependence of the grid array impedance is relevant on the E-plane since the impedance of the grid is angular dependent for TM polarization only. The angular dependence of the patch array impedance is instead relevant only on H plane (see relation (10)). An angular independent capacitive FSS is for instance an array of crosses [25, 26]. However, as it is evident from Fig. 6(b), the angular dependence of the capacitive FSS comprising the HIS has a weak influence on the H-plane radiation pattern since the presence of the varicap, which is angular independent, attenuates such dependency (see (10)).

4. FINITE SIZE ANTENNA

The analysis through the transmission line equivalent presented across the paper is useful for understanding the radiation principles of the structure but it is valid only for an infinite structure. As it is easy to understand, the size of a real antenna is necessary finite and the maximum gain of the structure depends on the aperture of the antenna.

In this section, the analysis of a finite structure is accomplished by a full-wave code, (Ansoft HFSS v.11). The parameters of the structure are the ones mentioned in the previous section and the size of the antenna is 33 cm × 33 cm × 1.9 cm. The aperture of the antenna is roughly $3.5\lambda_0$ at 3.3 GHz but it corresponds to $2.2\lambda_0$ at 2 GHz. The cavity height at the minimum operating frequency is roughly $\lambda_0/7$ and is smaller for lower frequencies.

The excitation of the cavity can be accomplished by a simple short dipole, by a wideband elliptical dipole [27] or alternatively by a printed patch antenna. It has to be pointed out that, if the polarization of the diode is changed and the operating frequency of the cavity is lowered, the dipole becomes much smaller than the original half-wavelength dimension.

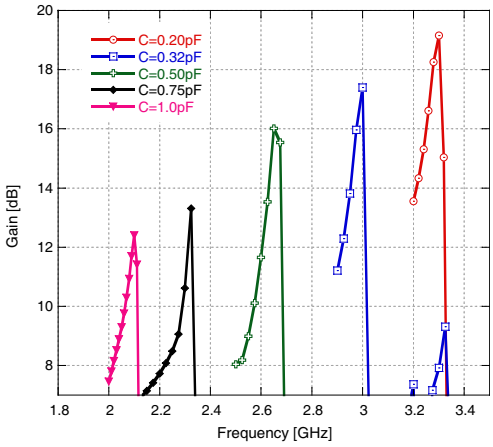

Figure 7. Gain towards the broadside direction by varying diode capacitances.

In Fig. 7, the maximum gain of the finite size antenna is reported as a function of the diode capacitances. A good agreement with the TL approach is observed with respect to the tuning range. The decrease of the gain is due to the reduction of the antenna effective area when the operating frequency is reduced. In Fig. 8, the radiation patterns on E and H planes are reported for some of the directivity maxima. As it is evident, at these frequencies, the antenna radiates towards broadside direction. The radiation patterns in correspondence of the directivity maxima are pencil beam.

The beam steering can be obtained in correspondence of every frequency by simply varying the diode capacitance around the value that generates the broadside pattern. In Fig. 9, the steering of the

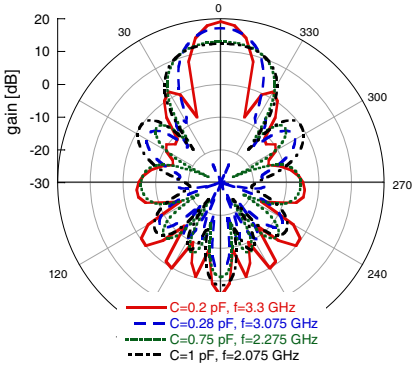

(a)

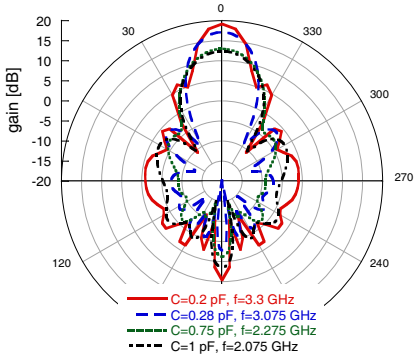

(b)

Figure 8. Radiation patters on (a) E-pane and (b) H-plane in correspondence of the of the directivity maxima for different capacitances.

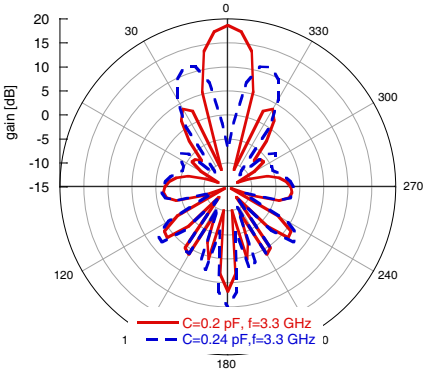

(a)

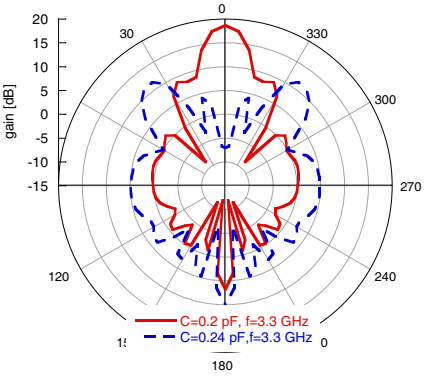

(b)

Figure 9. Radiation pattern at 3.3 GHz on (a) E-plane and (b) H-palne obtained by varying diode capacitances.

beam is shown at 3.3 GHz. As expected, by slightly varying the value of the capacitor, the main beam is split in both planes giving rise to a deep null towards the broadside direction. This property, other than frequency reconfigurability, is applicable for synthesizing smart antennas to Software Defined Radio (SDR) and Cognitive Radio applications [28–30]. In SDR applications, from the antenna design perspective, it is necessary to have a wideband coverage and a high level of reconfigurability. In cognitive radio applications, it is often assumed that the primary systems do not tolerate any interference from the secondary systems, i.e., the interference temperature constraints

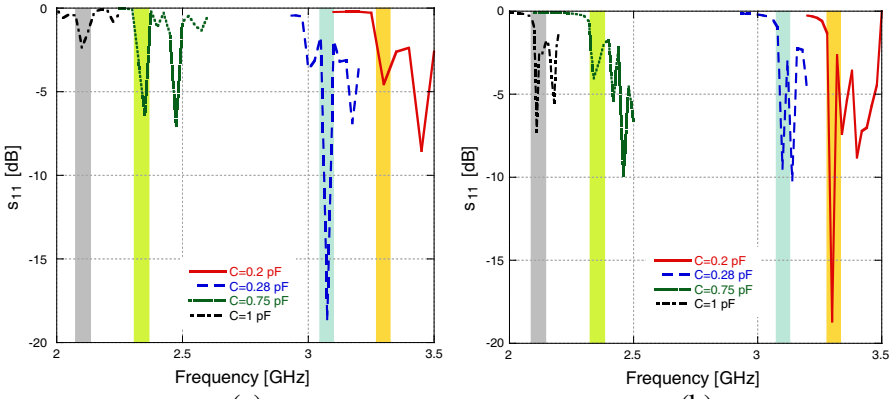

Figure 10. (a) S_{11} of the short dipole antenna and (b) of the elliptical dipole antenna as a function of the diode capacitance for the working frequencies of the cavity.

(ITCs) are fixed to be zero. In this case, the constraints are called null-shaping constraints [29].

Finally, the matching of the dipole antenna exciting the cavity is discussed. In Fig. 10, the source matching across all the frequency range is shown both in the case of a simple dipole of 44 mm and when the feeding source is a wideband elliptical dipole. The wideband dipole is matched across the overall frequency range when employed in freestanding case and it is characterized by a length of 60 mm and, according to the design in [27], a ratio of minor to major axis of 150%. In both cases the matching of the source is obtained since the Fabry-Perot cavity determines a sharp transition on the input impedance of the dipole at the resonance [23]. The use of the wideband dipole is preferable since it allows obtaining a better matching as opposed to the narrow band one. In order to reduce the mismatching losses of the antenna, a printed patch antenna or alternatively, a tunable primary radiator (e.g., tunable patch antenna) can be employed [16].

5. CONCLUSION

A tunable Fabry-Perot antenna, consisting of a dipole placed within a subwavelength cavity formed by a tunable HIS ground plane and a PRS superstrate has been analyzed using an equivalent transmission line model. The use of an active HIS allows both tuning the frequency of maximum broadside gain and obtaining a beam steering and beam shaping for a fixed frequency. The results obtained by the

equivalent transmission line model have been then verified by full-wave simulations on a finite size antenna.

ACKNOWLEDGMENT

Filippo Costa wishes to thank Dr. Olli Luukkonen, and Prof. Sergei Tretyakov for helpful discussions.

REFERENCES

1. Trentini, G. V., "Partially reflecting sheet arrays," *IRE Trans. Antennas Propagation*, Vol. 4, 666–671, 1956.
2. Lovat, G., P. Burghignoli, and D. R. Jackson, "Fundamental properties and optimization of broadside radiation from uniform leaky-wave antennas," *IEEE Trans. Antennas Propag.*, Vol. 54, 1442–1452, May 2006.
3. Neto, A. and N. Llombart, "Wideband localization of the dominant leaky wave poles in dielectric covered antennas," *IEEE Antennas and Wireless Propagation Letters*, Vol. 5, No. 1, 549–551, Dec. 2006.
4. Swillam, M. A., R. H. Gohary, M. H. Bakr, and X. Li, "Efficient approach for sensitivity analysis of lossy and leaky structures using FDTD," *Progress In Electromagnetics Research*, Vol. 94, 197–212, 2009.
5. Kim, D. and J.-I. Choi, "Analysis of a high-gain Fabry-Perot cavity antenna with an FSS superstrate: Effective medium approach," *Progress In Electromagnetics Research Letters*, Vol. 7, 59–68, 2009.
6. Sternberg, N. and A. I. Smolyakov, "Resonant transparency of a three-layer structure containing the dense plasma region," *Progress In Electromagnetics Research*, Vol. 99, 37–52, 2009.
7. Jackson, D. R. and A. A. Oliner, "A leaky-wave analysis of the high gain printed antenna configuration," *IEEE Trans. Antennas Propagation*, Vol. 36, No. 7, 905–910, 1988.
8. Feresidis, A. P., G. Goussetis, S. Wang, and J. C. Vardaxoglou, "Artificial magnetic conductor surfaces and their application to low profile high-gain planar antennas," *IEEE Trans. Antennas Propag.*, Vol. 53, No. 1, 209–215, Jan. 2005.
9. Yousefi, L., H. Attia, and O. M. Ramahi, "Broadband experimental characterization of artificial magnetic materials based on a microstrip line method," *Progress In Electromagnetics Research*, Vol. 90, 1–13, 2009.

10. Zhou, L., H. Li, Y. Qin, Z. Wei, and C. T. Chan, "Directive emissions from subwavelength metamaterial-based cavities," *Applied Physics Letters*, Vol. 86, 101101, Feb. 2005.
11. Kelly, J. R., T. Kokkinos, and A. P. Feresidis, "Analysis and design of sub-wavelength resonant cavity type 2-D leaky-wave antennas," *IEEE Trans. Antennas Propagation*, Vol. 56, No. 9, 2817–2825, 2008.
12. Zhao, J., Y. C. Jiao, F. Zhang, and X. Yang, "High gain circularly polarized antenna using sub-wavelength resonant cavity," *Journal of Electromagnetic Waves and Applications*, Vol. 24, No. 1, 33–40, 2010.
13. Costa, F., A. Monorchio, S. Talarico, and F. M. Valeri, "An active high impedance surface for low profile tunable and steerable antennas," *IEEE Antennas and Wireless Propagation Letters*, Vol. 7, 676–680, 2008.
14. Luukkonen, O., C. R. Simovski, A. V. Räisänen, and S. A. Tretyakov, "An efficient and simple analytical model for analysis of propagation properties in impedance waveguides," *IEEE Trans. on Microwave Theory and Techniques*, Vol. 56, No. 7, 1624–1632, 2008.
15. Weily, A. R., T. S. Bird, and Y. J. Guo, "A reconfigurable high-gain partially reflecting surface antenna," *IEEE Trans. on Antennas and Propagation*, Vol. 56, No. 11, 3382–3390, Nov. 2008.
16. Costa, F., E. Carrubba, A. Monorchio, and G. Manara, "Multi-frequency highly directive Fabry-Perot based antenna," *Proc. IEEE International Symposium on Antennas and Propagation*, 4–8, San Diego, CA, 2009.
17. Aydın, E., "Computation of a tunable slot-loaded equilateral triangular microstrip antenna," *Journal of Electromagnetic Waves and Applications*, Vol. 23, No. 14–15, 2001–2009, 2009.
18. Wu, X. H., A. A. Kishk, and A. W. Glisson, "A transmission line method to compute the far-field radiation of arbitrarily directed Hertzian dipoles in multilayer dielectric structure: Theory and applications," *IEEE Trans. on Antennas and Propagation*, Vol. 54, No. 10, 2731–2741, 2006.
19. Luukkonen, O., C. Simovski, G. Granet, G. Goussetis, D. Lioubtchenko, A. V. Räisänen, and S. A. Tretyakov, "Simple and accurate analytical model of planar grids and high-impedance surfaces comprising metal strips or patches," *IEEE Trans. on Antennas and Propagation*, Vol. 56, No. 6, 1624–1632, 2008.
20. Zhao, T., D. R. Jackson, J. T. Williams, H. D. Yang, and A. A. Oliner, "2-D periodic leaky-wave antennas — Part I:

Metal patch design," *IEEE Trans. Antennas Propagation*, Vol. 53, No. 11, 3505–3514, 2005.

21. Tretyakov, S., *Analytical Modelling in Applied Electromagnetics*, Artech House, Boston, 2003.
22. Costa, F., A. Monorchio, and G. Manara, "Analysis and design of ultra thin electromagnetic absorbers comprising resistively loaded high impedance surfaces," *IEEE Trans. on Antennas and Propagation*, Vol. 58, No. 5, 1551–1558, 2010.
23. Vu, T.-H., S. Collardey, A.-C. Tarot, and K. Mahdjoubi, "Input impedance of Fabry-Perot, EBG and leaky-wave antennas excited by a line source," *IEEE Antennas and Wireless Propagation Letters*, Vol. 8, 248–252, 2009.
24. Pirhadi, A., M. Hakkak, and F. Keshmiri, "Using electromagnetic bandgap superstrate to enhance the bandwidth of probe-fed microstrip antenna," *Progress In Electromagnetics Research*, Vol. 61, 215–230, 2006.
25. Zhang, J. C., Y. Z. Yin, and S. F. Zheng, "Double screen FSSs with multi-resonant elements for multiband, broadband applications," *Journal of Electromagnetic Waves and Applications*, Vol. 23, No. 16, 2209–2218, 2009.
26. Zhang, J.-C., Y.-Z. Yin, and J.-P. Ma, "Design of narrow bandpass frequency selective surfaces for millimeter wave applications," *Progress In Electromagnetics Research*, Vol. 96, 287–298, 2009.
27. Schantz, H. G., "Planar elliptical element ultra-wideband dipole antennas," *IEEE AP-S Int. Symp. Dig.*, Vol. 3, 44–47, San Antonio, TX, Jun. 2002.
28. Costa, F., A. Monorchio, and G. Manara, "Low-profile tunable and steerable Fabry-Perot antenna for software defined radio applications," *IEEE International Symposium on Antennas and Propag.*, Toronto, Canada, Jul. 11–17, 2010.
29. Haykin, S., "Cognitive radio: Brain-empowered wireless communications," *IEEE J. Sel. Areas Commun.*, Vol. 23, No. 2, 201–220, Feb. 2005.
30. Jorswieck, E. A. and R. Mochaourab, "Beamforming in underlay cognitive radio: Null-shaping constraints and greedy user selection," *Proc. CROWNCOM, 2010, 5th international Conference on Cognitive Radio Oriented Wireless Networks and Communications*, 1–5, Cannes, France, Jun. 9–11, 2010.